Exploration of Near-Field Structures of Aerated-Liquid Jets in a Quiescent Environment Using the X-Ray Technique

Kuo-Cheng Lin*
Taitech, Inc.
Beavercreek, Ohio 45430

Christopher Rajnicek, Jonathan McCall, Campbell Carter
Air Force Research Laboratory, Propulsion Directorate
Wright-Patterson AFB, Ohio 45433

Kamel Fezzaa
Argonne National Laboratory
Chicago, Illinois 60439

ABSTRACT

The structures of two-phase mixtures inside aerated-liquid (or effervescent) injectors and the structures of aerated-liquid jets discharged from specially contoured exit adaptors were experimentally explored, using the x-ray phase contrast imaging technique available at the Argonne National Laboratory. Water and nitrogen were used as the injectant and aerating gas, respectively. The study of internal two-phase flow structures showed that the present liquid aerator design generates a "homogeneous-like" internal two-phase mixture at a modest aeration level, due to vigorous mixing between the high-speed liquid flow and the tangentially-injected gas streams within a highly confined mixing region. High injection pressure within the injector body can suppress the expansion of the aerating gas and retard the mixing between liquid and aerating gas. In the study of the external spray structures, it was found that the exit adaptor with a constant or convergent flow passage generates a highly dispersed aerated-liquid spray. The aerated two-phase mixture injected through a convergent-divergent (C-D) flow passage experiences a continuous expansion process, resulting in an accelerated flow and a reduced pressure gradient between the discharged jet and the ambient air for a smaller lateral dispersion. The spray cone angle of an aerated-liquid jet injected through a C-D flow passage is relatively insensitive to the aeration level. Except for a very dense region where object overlap occurs along the projected line-of-sight path, droplets and gas bubbles can be identified from the x-ray images for size measurement. A highly-dispersed aerated-liquid jet can quickly generate a fairly uniform droplet size distribution within the near-field region of the spray, indicating that the atomization process is almost completed inside the injector adaptor. For the conditions examined, droplet SMD, bubble SMD and bubble film thickness are approximately 20, 40 and 10 μm, respectively.

*Corresponding author, Kuo-Cheng.Lin@wpafb.af.mil

INTRODUCTION

Liquid jet atomization plays an important role in establishing stable and efficient combustion inside the combustor of a liquid-fueled air-breathing propulsion system. For applications requiring both deep fuel penetration into high-speed crossflows for broader fuel spreading and smaller droplets in the liquid spray for faster evaporation, a superior liquid injection scheme must be sought. Among the possible candidates, aerated-liquid (or effervescent, or barbotage) jets have been explored extensively. It has been shown that the liquid aeration technique can generate a spray that penetrates well into the flow and produces a large fuel plume containing a large number of small droplets [1,2]. The required amount of aerating gas and delivery pressure are manageable for a high-speed air-breathing propulsion system. The utilization of aerated-liquid jets has led to successful combustion in a liquid-fueled high-speed air-breathing combustor [3].

While macroscopic and far-field features of the aerated-liquid jets have been extensively examined, detailed near-field spray structures cannot easily be explored, due to instrumentation difficulties. The relatively dense spray structure of an aerated-liquid jet prohibits the use of conventional shadowgraph imaging and or a phase Doppler particle analyzer (PDPA). The holographic technique exhibits limited success in measuring droplet size and velocity in the vicinity of the near-field jet [4]. Recently, the x-ray imaging technique available at the Argonne National Laboratory was successfully utilized to characterize dense diesel sprays [5,6] and aerated-liquid jets [7].

The study of Lin et al. [7] shows that highly convoluted wrinkle structures on the column surface of a turbulent pure-liquid jet can be observed by the x-ray phase contrast imaging technique. These wrinkle structures resemble turbulent eddies that have been shown in numerical simulations [8]. For a liquid jet with a modest aeration level, quickly-dispersed droplets and ligaments within the near field of the spray were visualized in the x-ray images. The observed spray structures do not, however, resemble the co-annular flow structures depicted by several previously published studies [9-12]. Never-before-seen entrained gas bubbles inside droplets and ligaments of aerated-liquid jets were also observed in the x-ray images. Quantitative measurement of droplet size, however, was not carried out in this study.

The objective of the present study is to experimentally investigate the structures of two-phase mixtures inside the aerated-liquid injector and the near-field structures of aerated-liquid jets injected through several specially contoured adaptors into a quiescent environment, using the phase contrast imaging technique combined with the x-ray source at the Argonne National Laboratory. The present study also intends to identify objects of interest, such as droplets and bubbles, from the line-of-sight x-ray images and then measure droplet diameter, bubble diameter, and bubble film thickness under various injection conditions.

EXPERIMENTAL METHODS

The experiment was conducted at the XOR 32-ID beamline of the Advanced Photon Source (APS) at Argonne National Laboratory. The undulator source provides the high x-ray brilliance necessary for the white-beam ultra-fast imaging technique. With the undulator gap set to 31 mm, most of the intensity was located within the first harmonic at 13.3 keV, with a peak irradiance of 10^{14} ph/s/mm^2/0.1%bw and a natural 5 bandwidth of 0.3 keV FWHM. For imaging of the liquid jet, the higher order harmonic was used and the lower energy was filtered with a 10 mm thick silicon slab. A fast scintillator crystal (LYSO:Ce, with a 40 ns decay time) converted the transmitted x-rays into visible light (434 nm). The images were captured with a CCD camera (Sensicam HS-SVGA, 1024×1280 pixels, from Cooke Corp.) coupled to the scintillator via a microscope objective (5x, NA=0.14) and a 45º mirror. The field of view of the imaging system (1.3 × 1.7 mm^2) matched the full usable x-ray beam size. The ultrafast imaging capability of the present setup provides an exposure time of 170 ps for each image.

Water and nitrogen were supplied into the aerated-liquid injector at desired flow rates to form a two-phase mixture in the injector before discharge into a quiescent environment. In order to investigate the two-phase mixture inside the aerated-liquid injector, two rectangular aerated-liquid injectors equipped with diamond windows at various locations along the injector axis were designed and fabricated. Figure 1 shows injector assembly and cross-sectional schematic. The internal flow path has a dimension of 1.0 mm (W) × 1.0 mm (D) × 64.0 mm (L) and is designed for liquid flow from the top. Two manifolds supply aerating gas from both sides of the rectangular injector. Aerating gas is injected into the liquid flow path through a total of 16 small orifices within the mixing region to generate two-phase mixture. Eight 178 μm aerating orifices are positioned on each side wall, as illustrated in Fig. 1(b).

A total of five diamond window pairs, two pairs for one injector and three pairs for the other injector, with a viewable diameter of 2.8 mm are strategically positioned along the injector axis for the investigation of the two-phase mixture evolution. Single crystal synthetic diamond film with a thickness of 0.3 mm provides high x-ray transmittance. Injection pressures for liquid and aerating gas are measured through the pressure taps shown in Fig. 1. An adaptor with a flow

passage dimension of 0.75 mm (W) × 0.75 mm (D) can be attached to the end of the rectangular injector, in order to raise the injection pressures. Because the flow passage is square, the external spray structure generated from this injector configuration is not the focus of this study.

For the study of external spray structure, an axisymmetric aerated-liquid injector with an exit diameter of 2.0 mm was designed. This injector has a liquid/gas mixing scheme similar to the one shown in Fig. 1. An adaptor with a specific internal contour, as shown in Fig. 2, can be mounted at the injector exit to provide the desired transition from the 2.0 mm injector exit to a throat diameter of 1.0 mm (except for Configuration #5). Table 1 lists the selected internal contours. These contour profiles provide additional means to modify the two-phase mixture, through, for example, pressure variation and cavitation, before the mixture discharges into a quiescent environment. Two sets of adaptors with lengths of 2.5 mm (L/D=2.5, D=1.0 mm) and 10.0 mm (L/D=10, D=1.0 mm) were tested to explore the effects of passage length and contour curvature on spray structure.

The aerated-liquid jet was vertically discharged into a collecting bucket with a small opening on the cap to prevent drifted droplets from getting into the beam path. In addition, the distance between the nozzle exit and the bucket cap was kept around 10 mm, in order to avoid splashing. Both the aerated-liquid injector and the collecting bucket were rigidly mounted on a traversing table, which provided movement normal to the x-ray beam.

RESULTS AND DISCUSSION

Evolution of Internal Two-Phase Mixtures

Figure 3 shows composite x-ray images to demonstrate the evolution of two-phase mixtures inside the rectangular injector at four injection conditions. Each composite image consists of three individual x-ray images taken at different time instances and corresponds to a total height of 2.4 mm and a width of 1.1 mm. Due to the limitations of fabricating perfectly perpendicular internal corners, the passage corner has a small radius, which appears as a gray band between the clear viewable flow passage and the dark injector metal body. Also, a slight misalignment of the injector with respect to the x-ray beam path can limit the viewable area of the diamond window. Consequently, the physical width of the clear viewable area is less than the 1.0 mm width of the flow passage. Finally, the flow structures close to the side walls are invisible with the present x-ray intensity setting. One of the diamond films near the injector exit cracked during the injector assembly process and was not replaced in the present study. Nonetheless, the remaining four window pairs provide valuable insights into the evolution of two-phase mixture from the beginning (Window #1) to the end (Window #4) of the mixing area inside the present rectangular injector.

Figure 3(a) shows the two-phase flow evolution for an injection condition with a relatively low liquid flow rate (Q_L=2.3 g/s) and a low aeration level (GLR=2%). Large gas bubbles/voids are generated from the first row of aerating orifices and stay close to the wall at the upstream location. No distinct small gas bubbles are generated, probably due to the lack of sufficiently high shear force from the liquid flow to overcome surface tension force or the effects of a relatively large aerating orifice. An intact liquid core still exists within the field of view of Window #1. The composite images from Windows #2 and #3 show that further addition of aerating gas from downstream aerating orifices promotes vigorous mixing between liquid and aerating gas. With the capability of x-ray phase contrast imaging, a two-phase mixture with small bubbles suspended in liquid, small droplets within gas voids, and wrinkled and overlapped interfaces between liquid and gas can be observed at this stage. Improved gas/liquid mixing is achieved at the further downstream locations. It is obvious that the internal flow is not bubbly at the time it emerges from the mixing area. Because the corners of the flow passage are slightly rounded, as mentioned previously, it cannot be concluded whether the final two-phase mixture is a co-annular flow. The resulting spray may exhibit limited liquid atomization.

The evolution of the internal two-phase mixture with an elevated aeration level of 8% at the same liquid flow rate is shown in Fig. 3(b). With more gas injected into the liquid flow path, impingement of the gas jets appears far upstream. The liquid injection pressure increases from 0.16 MPa for the condition in Fig. 3(a) to 0.30 MPa for the condition in Fig. 3(b). The intact liquid core terminates right at the first row of aerating orifices. No discrete gas bubbles are generated from the present injector design operated at this flow condition. Improved gas/liquid mixing can be clearly seen through Windows #2 and #3. Eventually, a two-phase mixture with a finer interfacial structure is generated at the exit of the mixing area. Judging from the line-of-sight x-ray image at Window #4 in Fig. 3(b), one cannot tell whether these fine interfacial structures are distributed within a “homogeneous-like” two-phase mixture or adhere to the surface of annular liquid films formed on the inner surface of the injector flow path and attached to the diamond windows.

Figure 3(c) shows the two-phase flow evolution with Q_L=13.6 g/s and GLR=2%. With a higher liquid flow rate to quickly bend the gas stream and a higher local pressure ($P_{inj,L}$=1.15 MPa) to suppress the gas volume, no gas pockets can be observed within the clear field of view of Window #1. The intact liquid core

persists even within the field of view of Window #3. Surprisingly, fine interfacial structures are quickly generated at the exit of the mixing area (Window #4). Pressure differences may cause preferential gas injection from the last rows of aerating orifices in the present injector design at this injection condition, as will be discussed later. Comparing to the composite image for Window #4 of Fig. 3(a), it appears that a well-mixed two-phase mixture is probably generated at the same aeration level of 2%, despite the relatively late occurrence of full duct mixing for this injection condition.

With a further increase in gas aeration level to 8% at Q_L=13.6 g/s, gas pockets stay close to the side walls within Window #1 in Fig. 3(d). A sudden and significant change in internal flow structure takes place within the first three rows of the aerating orifices. The intact liquid core can no longer be observed within Window #2. The two phase mixture further undergoes a refinement process through intensive liquid/gas mixing to exhibit very fine interfacial structures from Window #2 to Window #4.

Based on the observations so far, the primary working mechanism by which the present aerated-liquid injector design delivers better-atomized sprays comes from the vigorous mixing between liquid and aerating gas streams within a relatively confined space (1.0 mm × 1.0 mm) inside the injector. Generation of discrete gas bubbles cannot be achieved by the present design at GLR>2%. The present x-ray images cannot confirm whether the final two-phase mixture is a co-annular flow or not, due to the line-of-sight nature of the x-ray image and the rounded flow passage corners.

Figure 4 shows the simulated density contours inside an axisymmetric aerated-liquid injector. This figure is adopted from the study of Cassidy et al. [13]. The numerical simulation was performed inside a 1.0 mm injector with a mixing area configuration similar to the present study and an injection condition of Q_L=7.6 g/s and GLR=2%. As can be seen in Fig. 4, the simulated two-phase mixture exhibits a relatively long intact liquid core, similar to that observed in Fig. 3(c). The injected aerating gas mainly occupies the space along the injector wall. As it approaches the nozzle exit, the intact liquid core breaks up and mixes with the aerating gas to reach a two-phase mixture which is not in the form of co-annular flow. The co-annular flow structure with a core gas stream and a thin layer of squeezed liquid film along the nozzle wall has been the typical exit two-phase mixture observed in several studies on aerated-liquid (or effervescent) jets at a high aeration level [9-12]. For the two-phase mixture at the exit of the injector in Fig. 4, however, more liquid mass may be distributed along the injector axis, since the majority of the aerating gas stays close to the injector wall. Combining this numerical result with the x-ray images within Window #4 of Figs. 3(b)-3(d), one can clearly see that a "homogeneous-like" two-phase mixture can be generated by the present injector design operated at adequate injection conditions, provided further mixing can be achieved between the liquid-dominated central core and the gas-dominated periphery region. This additional mixing could possibly be achieved through the use of a long mixing tube or a specially contoured adaptor.

Effects of Pressure on Internal Two-Phase Mixtures

With the present design concept for an aerated-liquid injector, the structure of the final two-phase mixture prior to discharge depends on controllable parameters, such as mixing area configuration, liquid flow rate, and aeration level, as well as inherent parameters, such as local pressure and void fraction. As can be seen on a comparison of Figs. 3(a) and 3(c), the commonly used aeration parameters, such as GLR in the present study, fall short of accurately indicating the two-phase mixture before the nozzle exit. While characterizing the final structure of the two-phase mixture is a complicated task, the present study highlights the effects of local pressure on the structure of internal two-phase flows.

Figure 5 shows composite x-ray images obtained from two window locations to illustrate the effect of injection pressure on two-phase mixtures inside the rectangular injector. An adaptor with a passage dimension of 0.75 mm × 0.75 mm can be attached to the exit (1.0 mm × 1.0 mm) of the rectangular injector to restrict the two-phase flow discharge. Higher injection pressures for both liquid and aerating gas are, therefore, required to achieve the flow rates of an unrestricted flow. For the test conditions in Fig. 5, liquid flow rate and aeration level were kept at Q_L=13.6 g/s and GLR=4%, respectively.

With an unrestricted flow in Fig. 5(a), the intact liquid core appears to end within the field of view of Window #2. A two-phase flow with fine interfacial structures is generated at the downstream Window #4 location. With the same bulk flow rates for liquid and aerating gas for the restricted flow in Fig. 5(b), however, the intact liquid core persists within the field of view of Window #2, because gas expansion is suppressed at a high local pressure. Consequently, the void fraction is smaller for the restricted flow in Fig. 5(b) than that within the unrestricted flow in Fig. 5(a) at the Window #2 location. With limited mixing between liquid and aerating gas in the upstream region of the mixing area, the two-phase mixture of the restricted flow exhibits large-scale filament-like interfacial structures within the Window #4 location. Judging from the internal flow structure alone, it is expected that the resulting spray of the restricted flow may generate large and congregated droplets. The injected sprays from

both conditions of Fig. 5 were not explored in the present study, due to the change in exit dimension introduced by the adaptor. Nonetheless, the study in Fig. 5 clearly highlights the effect of local pressure on the structure of the internal two-phase flow of an aerated-liquid injector. An injector design requiring a lower injection pressure may ease the operational requirements.

Figure 6 from Cassidy et al. [13] shows the pressure profile inside an axisymmetric aerated-liquid injector at various aeration levels. A pressure probe with an OD of 152 μm and an ID of 50 μm was inserted from upstream of a 1.0 mm aerated-liquid injector, which has a mixing area similar to that used in the present study. The presence of the pressure probe will inevitably change the flow characteristics inside the injector, but these pressure profiles can still provide useful insights into the mixing process inside the injector.

As can be seen in Fig. 6, no significant pressure drop takes place in the two-phase flow path until the downstream section of the mixing area. With a high injection pressure inside the gas manifold to ensure gas flow into the liquid, the pressure gradient between the aerating gas and the two-phase flow increases toward the downstream section of the mixing area. With the same aerating orifice diameter and the given distribution pattern for the aerating orifice, as depicted in Fig. 1, preferential injection of the aerating gas into the liquid flow, therefore, exists along the flow path. More gas will be injected from the downstream section of the mixing area, resulting in a sudden change in the structure of the two-phase flow, as observed between Window #3 and Window #4 in Fig. 3(c) and between Window #1 and Window #2 in Fig. 3(d). Figure 6 also shows that the pressure drop within the two-phase flow path increases as the liquid aeration level increases. Consequently, the degree of preferential gas injection in the two-phase flow path increases as the liquid aeration level (or injection pressure) increases. Changes in the mixing area design may mitigate this issue.

Effects of Adaptor Contours

Pure-Liquid Jets:

Figure 7 shows composite x-ray images of pure-liquid jets discharged from various adaptors (see Fig. 2) attached to a 2.0 mm aerated-liquid injector. These composite images have been digitally processed by histogram normalization to enhance the contrast ratio, so that interference from the background noise can be minimized and the interfaces of objects with a small field of depth, such as small droplets and ligaments, can be clearly visualized. This contrast enhancement process, however, gives up the sense of thickness in the line-of-sight direction. An object with a darker shade typically possesses a greater thickness in the unprocessed x-ray image. Also shown in Fig. 7 is the adaptor throat diameter, marked as a red line at the top of each composite image. The adaptor passage length is 10 mm (L/D=10). Configuration #2 was not tested in the present study, due to time constraints. The liquid flow rate was kept at 18.2 g/s, resulting in a flow Reynolds number based on the throat diameter of 22.9×10^3 (45.8×10^3 for the Configuration #5 adaptor).

At this liquid flow rate, the discharged jet appears as a typical turbulent liquid jet for the Configuration #1 adaptor in Fig. 7(a). As previously observed, wrinkle structures on the jet surface, resembling turbulent eddies, are clearly depicted by the x-ray phase contrast imaging technique [7]. Some gas bubbles can also be observed within the liquid column.

Surprisingly, the jet structure out of the Configuration #3 adaptor is highly unsteady, and a composite spray image representing a continuous spray structure could not be constructed from the obtained individual images, as illustrated in Fig. 7(b). The jet exhibits a jet width greater than the throat diameter with an oscillatory motion along the jet axis. Comparing with Fig. 7(a), more gas bubbles are embedded inside the highly unsteady liquid jet, probably due to liquid cavitation. Fairly large drops are generated. The recirculation zone between the liquid surface and the divergent section of the adaptor surface may exhibit unsteadiness and, subsequently, affect the jet structure. The possibility that the contour surface of this adaptor was not perfectly fabricated cannot be ruled out as the contributing factor for the observed unsteady spray at this point.

The liquid jet out of the Configuration #4 adaptor initially appears as a laminar jet in Fig. 7(c), due to the suppression of turbulent eddy growth within the boundary layer by the continuous convergent wall in the adaptor. Wrinkle structures appear about one diameter length downstream. Unlike the liquid jet in Fig. 7(a), there are no gas bubbles within the liquid column for this adaptor configuration, which appears to be least able to break up the liquid jet.

Figure 7(d) shows the liquid jet discharged from the Configuration #5 adaptor. The 0.5 mm throat diameter generates a higher jet exit velocity. Several interesting features can be observed in this liquid jet. First, small droplets are generated very close to the adaptor exit, as illustrated in the zoom-in box in Fig. 7(d), indicating that the liquid breakup process takes place inside the adaptor. Second, small ligaments are quickly generated in the field of view. These ligaments are roughly aligned with the jet axis. Third, small gas bubbles are entrained inside the ligaments, as illustrated in the zoom-in box in Fig. 7(d), due to liquid cavitation taking place downstream from the adaptor throat. Bubble bursting cannot be observed within the field of view and is believed to take place further downstream

to break up the ligaments and generate small droplets. Fourth, the overall jet width is slightly larger than the throat diameter at the adaptor exit plane. The widening of the jet width may come from the expansion of gas bubbles due to cavitation and from the separation of ligaments from the liquid core. Fifth, this liquid jet does not exhibit dramatic oscillatory motion, probably due to its relatively high exit velocity. Finally, several large drops appear in the composite image. These drops are generated from the liquid buildup attached to the adaptor exit plane, as can be seen at the top of the composite image in Fig. 7(d). The recirculation zone between the liquid surface and the divergent section of the adaptor surface assist in the liquid buildup.

The liquid jet discharged from the Configuration #6 adaptor appears to tilt toward the left side of the composite image in Fig. 7(e). This jet appearance may be caused by an imperfection in the adaptor internal contour (i.e., the convergent angle of this adaptor contour may not have been machined uniformly). The resulting jet width is greater than the throat diameter. A smaller liquid core, which may not be clearly visualized in Fig. 7(e) due to the contrast enhancement process, aligns with the jet axis. Despite the abnormal jet appearance, this adaptor was utilized for the study of aerated-liquid jets.

Aerated-Liquid Jets:

Figure 8 shows contrast-enhanced composite x-ray images of aerated-liquid jets discharged from the same adaptors at the same liquid flow rate. The liquid aeration level was kept at 2%. Also shown on each composite image are throat diameter (red line), exit orifice diameter (blue line, if different from the throat diameter), jet axis (white chain line), and the estimated jet boundary (yellow dot line).

Comparing with the corresponding pure-liquid jet structure in Fig. 7, it is obvious that the modestly-aerated liquid jet is significantly dispersed and has no observable intact liquid core for all five adaptor configurations. Fine droplets, small ligaments, and tiny bubbles are generated upon discharging. The capability of the x-ray phase contrast imaging technique facilitates the observation of these objects, especially within the less dense regions of the spray. Unlike the observations for pure-liquid jets in Fig. 7, the potential effects of fabrication-related contour imperfections appear to be minimal for the aerated-liquid jets, as shown in Fig. 8. Regardless of the effects of the adaptor contours on spray structure, the observed spray structure close to the adaptor exit can be linked to the fine interfacial structure of the internal two-phase flow near the nozzle exit, as observed in Fig. 3. No structure resembling a thin liquid film can be observed at the adaptor exits in Fig. 8. This observation indicates that the discharged two-phase flow is a "homogeneous-like" mixture, not a co-annular flow as observed in some studies [9-12]. The vigorous mixing between liquid flow and tangentially injected aerating gas within a confined space thus appears to be an effective strategy in liquid atomization.

Figure 8 also shows that, if properly aerated, the majority of the liquid atomization process is completed by the time the two-phase mixture exits the adaptor orifice. Subsequent two-phase flow dispersion to form a specific spray cone is dictated by the injection pressure and the adaptor contour. Unfortunately, the injection pressures for these five injection conditions were not recorded for comparison. The Configuration #5 adaptor does require a higher injection pressure, due to its smaller throat diameter for the same liquid flow rate and aeration level. If the spray structure discharged from the Configuration #1 adaptor is selected as the reference, it is obvious that the spray structures generated from the Configuration #3, #5, and #6 adaptors exhibit smaller spray cone angles. The aerated-liquid jet discharged from the Configuration #5 adaptor in particular does not expand to fill the entire adaptor exit orifice. The prescribed exit divergent angles of these three adaptors with convergent-divergent (C-D) contours do not appear to enhance the jet spreading angle. Instead, the exit spreading angles for jets discharged from the Configuration #3 and #6 adaptors closely match the machined exit slopes of both adaptors.

The "homogeneous-like" two-phase mixture, which behaves like a compressible gas, expands continuously through the C-D contour, resulting in a reduced pressure drop across the exit plane for further lateral expansion and an increased exit velocity. As with the compressible gas flow, the internal two-phase flow reaches the sonic speed of the local two-phase mixture and, therefore, chokes at the adaptor throat. The two-phase mixture further experiences a continuous pressure drop before reaching the adaptor exit and loses its ability to expand laterally upon discharging. These narrow high-velocity "porous" liquid jets may potentially possess sufficiently high momentum fluxes (ρu^2) for additional penetration into a high-speed crossflow, with the trade-off of less lateral dispersion. The porosity of the two-phase mixture due to entrained aerating gas and cavitation may contribute to easy breakup processes further downstream.

The intended objective of exploring the effects of liquid cavitation, provided by the C-D contour, on atomization enhancement, however, cannot be carried out within the field of view of the #3, #5, and #6 sprays shown in Fig. 8, due to the highly congregated two-phase mixture, the line-of-sight feature of the x-ray images, and the existing embedded gas bubbles from liquid aeration.

The spray discharged from the Configuration #4 adaptor exhibits the largest cone angle among the five jets. The continuously convergent contour of the Configuration #4 adaptor ensures that the two-phase mixture can only be choked at the adaptor exit. For the Configuration #1 adaptor, choking of the two-phase flow typically takes place slightly downstream of the contoured transition section at the adaptor entrance, due to flow separation. Nonetheless, both the Configuration # 1 and #4 adaptors generate highly dispersed sprays, allowing for a close examination of the spray structures. Well-separated fine droplets and bubbles are distributed within the majority of the spray volume. In addition, fine filament-like structures are sparsely distributed within both sprays, as depicted in the zoom-in boxes in Figs. 8(a) and 8(c). This observation highlights the difficulty of achieving a truly homogeneous two-phase mixture with the present mixing configuration design. Improvements may be made with optimization of diameter, number, and arrangement of aerating orifices.

As the aeration level is further increased to 4% at the same liquid flow rate, the macroscopic spray appearance of each spray remains similar, as can be seen in Fig. 9. The same aeration level, however, could not be reached for the Configuration #5 adaptor, due to its small throat diameter and pressure constraints of the flow meters. The spray cone angles for jets discharged from the Configuration #1 and #4 adaptors exhibit further increases due to the increase in aeration level. The number and length scale of fine-filaments reduce for both sprays, indicating that better-homogenized two-phase mixtures are generated within the injector, as the aeration level increases. Of course, both adaptor configurations minimize the pressure drop across the given adaptor length and generate a large lateral dispersion to further unify droplet spatial distribution.

There is a small increase in jet lateral spreading for the aerated-liquid jets discharged from the Configuration #3 and #6 adaptors, as the aeration level increases from 2% to 4%. The continuous expansion process across the C-D adaptors does an efficient job of maintaining a big pressure drop across the given adaptor length. Without a large lateral dispersion to tear apart the homogenized two-phase mixtures, fine liquid filaments and bubble-embedded ligaments are still present within the discharged sprays, as illustrated in the zoom-in boxes in Figs. 9(b) and 9(d).

In summary, the macroscopic spray structures of aerated-liquid jets discharged from the selected adaptor configurations show that an adaptor with a straight or a continuous convergent contour generates a highly-dispersed spray containing well-atomized fine droplets. The adaptor with a C-D contour, however, produces a relatively confined spray cone with a high exit velocity. The effect of cavitation could not be easily explored within the near field of an aerated-liquid jet.

Droplet Size Measurement for Aerated-Liquid Jets

The present study attempts to quantify the droplet size within the near-field of aerated-liquid jets, using digitally enhanced x-ray phase contrast images. An in-house code was developed to identify objects of interest, i.e., droplets and bubbles, and then to measure their equivalent outside diameters and mean bubble film thickness. Entrained gas within droplets (or gas bubbles) can be clearly visualized with the present imaging technique, as illustrated in Fig. 10(a). These bubbles can be easily misidentified as relatively large droplets in conventional shadowgraph images. Since the x-ray phase contrast imaging technique captures the spray features along the line-of-sight, overlap among objects of interest in the resulting image is likely within the near-field region. No attempt was made to resolve this issue in the present study. Outer boundaries of the x-ray image were cropped so that the size measurement was only conducted within a high-intensity, high-contrast region. The cropped image was further divided into 15 sub-grids. Each resulting sub-grid has a height of 342 μm and a width of 274 μm, representing a refined resolution in probing the spray structure (within the line-of-sight). Spatial location of the identified objects is based on the centroid coordinates.

Figure 10 (a) shows an image taken on the outskirt of an aerated-liquid jet with the objects of interest identified and color-marked by the in-house code. Within this region of the spray (x=7.0 mm and r=4.2 mm for the center of the image), the droplet number density is relatively low and a fairly high percentage of objects can be confidently identified for size measurement. It was observed that large objects are more likely to overlap with nearby objects in the x-ray image and, consequently, may be ignored for size measurement. The reported droplet size distribution can, therefore, be affected by this bias. Measurements of bubble diameter and film thickness are affected more by this bias, since most of the overlapped objects involve large gas bubbles. Furthermore, as a side effect of the digital enhancement process, objects with an effective diameter of approximately 3.9 μm or less are ignored. This may further bias the size distribution measurements. Figure 10(b) shows an image taken close to the core of the spray (x=8.0 mm and r=0 for the center of the image). Here, the highly overlapping features make object identification nearly impossible and no size measurement can be made within this region.

The typical size distribution histogram for equivalent droplet diameter is shown in Fig. 11 for the test condition shown in Fig. 8(a). Within the probe volume with the center at x=7.0 mm and r=3.35 mm, a total of 345 objects were identified per sub-grid from a set of 10 images taken at the same injection condition and the same spatial location. Among them, there are

325 droplets and 20 gas bubbles. The total number of identified objects (for the set of 10 images) within each sub-grid varies from 50 to 350, depending on the probing location for this test condition. Figure 11 shows that a mono-dispersed droplet size distribution is typically generated for this spray. Fine droplets with a diameter in the 10-15 μm range, along with a few big drops with a diameter up to 35 μm, were measured. The calculated droplet SMD is 15.6 μm. Not shown in the figure is the bubble SMD, which is 36.1 μm. If these bubbles were misidentified as solid droplets, the overall SMD increases to 20.9 μm. The average bubble film thickness is 8.2 μm.

Figure 12 shows size distributions along axial (x direction) line-of-sight probing paths at three radial (r direction) locations of the same aerated-liquid jet. For this spray, droplet size within the spray core region with r<2.25 mm could not be measured, due to the high number density of droplets within the line-of-sight. As can be seen from the droplet SMD distribution in Fig. 12(a), a fairly uniform droplet size can be generated by the present liquid aeration technique, indicating that the droplet breakup process is completed less than 2 diameters (2.0 mm) downstream from the adaptor orifice exit or even within the adaptor, for this injection condition with the equipped adaptor. The droplet SMD is centered around 16 μm with a maximum slightly less than 20 μm.

The measured bubble SMD distributions in Fig. 12(b) do not exhibit strong evidence of bubble expansion toward the downstream locations of the spray within the present probing region. The relatively high scattering in the bubble SMD distribution in Fig. 12(b) comes from the limited number of bubbles within the probing volume. As discussed in relation to Fig. 11, less than 10% of the identified objects are gas bubbles. The averaged bubble SMD is around 40 μm, which is generally two times larger than the measured droplet SMD.

Figure 12(c) shows the mean thickness for the identified gas bubbles. Similar to the observation in Fig. 12(b), there is no strong evidence that there is any decrease in film thickness due to bubble expansion within the probing region. The average film thickness is around 8.5 μm. Combined with the average bubble SMD, the equivalent diameter of the gas void is around 23 μm.

Figure 13 shows similar plots along three radial probing paths at three downstream locations. This set of plots covers more peripheral regions of the spray. Similar to the observations of Fig. 12, there is no strong evidence to show size evolution for droplet SMD, bubble SMD, or film thickness within the probing region. With the line-of-sight feature of the x-ray image, this observation, once again, indicates that the droplet size is fairly uniform across the spray plume within the near field of the spray. Means to explore the dense core region, which is still indiscernible by the present x-ray phase contrast imaging technique, should be sought to further confirm this observation. Nonetheless, it is clear that droplet size is determined by the structure of the internal two-phase mixture for a well-dispersed aerated-liquid jet. Size distributions within sprays of other injection conditions will be reported in the future.

CONCLUSIONS

The structures of two-phase mixtures inside the aerated-liquid injectors and the structures of aerated-liquid jets discharged from specially contoured exit adaptors were experimentally explored, using the x-ray phase contrast imaging technique at the Argonne National Laboratory. Water and nitrogen were used as the injectant and aerating gas, respectively. Two rectangular aerated-liquid injectors equipped with diamond windows for x-ray access were designed for the exploration of internal two-phase mixtures. In addition, a 2 mm axisymmetric aerated-liquid injector equipped with an exit adaptor was utilized for the investigation of external spray structure. A total of six adaptors with various internal configurations and a reduced throat diameter of 0.5 or 1.0 mm were selected for testing. The major conclusions obtained of the present study are as follows:

For the study of the internal two-phase flow structures:

1. The present design concept for liquid aeration will not generate bubbly or co-annular flow inside the aerated-liquid injector. Instead, a “homogeneous-like” two-phase mixture can be generated at a modest aeration level.
2. It is believed that the “homogeneous-like” two-phase mixture is generated through vigorous mixing between the high-speed liquid flow and the tangentially-injected gas streams within a highly confined mixing region.
3. With an increase in liquid aeration level, the length scale of the interfacial structure of the two-phase flow decreases, indicating an increase in gas/liquid mixing.
4. An injection condition or an injector design, that requires a high injection pressure within the injector body, can suppress the expansion of the aerating gas and, consequently, retard the mixing process between liquid and aerating gas.
5. The present design concept for liquid aeration exhibits preferential gas injection along the mixing region with more gas injected into the liquid flow from the downstream section of the mixing area.

For the study of the external spray structures:

1. As Compared to the pure-liquid jet, the aerated-liquid jet is fairly insensitive to minor imperfections in the internal contours of the exit adaptor.
2. The exit adaptor with a constant or convergent flow passage generates a highly dispersed aerated-liquid spray, while the exit adaptor with a convergent-divergent (C-D) flow passage generates a narrow aerated-liquid spray. The lateral dispersion increases as the aeration level increases.
3. The aerated two-phase mixture injected through a C-D flow passage experiences a continuous expansion process, resulting in an accelerated flow and a reduced pressure gradient between the discharged jet and the ambient air for a smaller lateral dispersion.
4. The spray cone angle of an aerated-liquid jet injected through a C-D flow passage is relatively insensitive to the aeration level.
5. Except for a very dense region, where object overlapping occurs along the projected line-of-sight path, droplets and gas bubbles can be identified from the x-ray images for size measurement.
6. A highly-dispersed aerated-liquid jet can quickly generate a fairly uniform droplet size distribution within the near-field region of the spray, indicating that the atomization process is almost complete inside the injector adaptor.
7. For the conditions examined, droplet SMD, bubble SMD and bubble film thickness are approximately 20, 40 and 10 μm, respectively.

A significant amount of the data from this series of tests has not been fully analyzed. The effects of aeration level and adaptor configuration on droplet size distribution will be reported in the future.

ACKNOWLEDGEMENTS

This work was sponsored by the AFRL/Propulsion Directorate under contract number FA8560-08-D-2844 (Contract monitor: Robert Behdadnia). Use of the Advanced Photon Source at Argonne National Laboratory was supported by the U. S. Department of Energy, Office of Science, Office of Basic Energy Sciences, under Contract No. DE-AC02-06CH11357. The authors would like thank Matt Streby, Steve Enneking, and Timothy Bulcher (Taitech, Inc.) for their assistance in hardware design, setup, and data acquisition.

REFERENCES

1. Lin, K.-C., Kennedy, P. J., and Jackson, T. A., "Spray Structures of Aerated-Liquid Jets in Subsonic Crossflows," AIAA Paper 2001-0330, 2001.
2. Lin, K.-C., Kennedy, P. J., and Jackson, T. A., "Structures of Aerated Liquid Jets in High Speed Crossflows," AIAA Paper 2002-3178, 2002.
3. Mathur, T., Lin, K.-C., Kennedy, P., Gruber, M., Donbar, J., Jackson, T., and Billig, F., "Liquid JP-7 Combustion in a Scramjet Combustor," AIAA Paper 2000-3581, 2000.
4. Sallam, K. A., Aalburg, C., Faeth, G. M., Lin, K.-C., Carter, C. D., and Jackson, T. A., "Primary Breakup of Round Aerated-Liquid Jets in Supersonic Crossflows," *Atomization and Sprays*, Vol. 16, No. 6, 2006, pp. 657–672.
5. Wang, Y., Liu, X., Im, K.-S., Lee, W.-K., Wang, J., Fezzaa, K., Hung, David, and Winkelman, J., "Ultrafast X-Ray Study of Dense Liquid Jet Flow Dynamics Using Structure Tracking Velocimetry," *Nature Physics*, Vol. 4, 2008, pp. 305-309.
6. Qun, S., Lee, W-K., Fezzaa, K., Chu, Y. S., De Carlo, F., Jemian, P., Ilavsky, J., Erdman, M., and Long, G., "Dedicated Full-Field X-Ray Imaging Beamline at Advanced Photon Source," *NIM A* 582 (1), 77-79 (2007).
7. Lin, K.-C., Carter, C., Fezzaa, K., Wang, J., Liu, Z., "X-Ray Study of Pure- and Aerated-Liquid Jets in a Quiescent Environment," AIAA Paper 2009-0994, January 2009.
8. Pai, M., Pitsch, H., and Desjardins, O., "Detailed Numerical Simulations of Primary Atomization of Liquid Jets in Crossflow," AIAA Paper 2009-0373, January, 2009.
9. Kim, J. Y., and Lee, S. Y., "Dependence of Spraying Performance on the Internal Flow Pattern in Effervescent Atomizers," *Atomization and Sprays*, Vol. 11, 2001, pp. 735-756.
10. Lorcher M., Schmidt, F., and Mewes, D., "Effervescent Atomization of Liquids," *Atomization and Sprays*, Vol. 15, 2005, pp. 145-168.
11. Catlin, C. A., and Swithenbank, J., "Physical Processes Influencing Effervescent Atomizer Performance in the Slug and Annular Flow Regimes," *Atomization and Sprays*, Vol. 11, 2001, pp. 575-595.
12. Huang, X., Wang, X., and Liao, G., "Visualization of Two Phase Flow inside an Effervescent Atomizer," *Journal of Visualization*, Vol. 11, No. 4, 2008, pp. 299-308.
13. Cassidy, D. A., Choi, J., Tian, M., Edwards, J. R., and Lin, K.-C., "Numerical Simulation of Two-Phase Flow within an Aerated Liquid Injector," AIAA Paper 2010-0098, January 2010.

Table 1. Dimensions of the exit adaptor for the 2.0-mm axisymmetric aerated-liquid injector

Configuration	#1	#2[a]	#3	#4	#5[b]	#6
D1	2.0 mm	1.0 mm	2.0 mm	2.0 mm	2.0 mm	2.0 mm
D2 (throat)	1.0 mm	N/T	1.0 mm	1.0 mm	0.5 mm	1.0 mm

Note: a: Not tested. No rounded transition from 2.0 mm to 1.0 mm.
b: Throat diameter of 0.5 mm. GLR=4% could not be reached for this configuration.

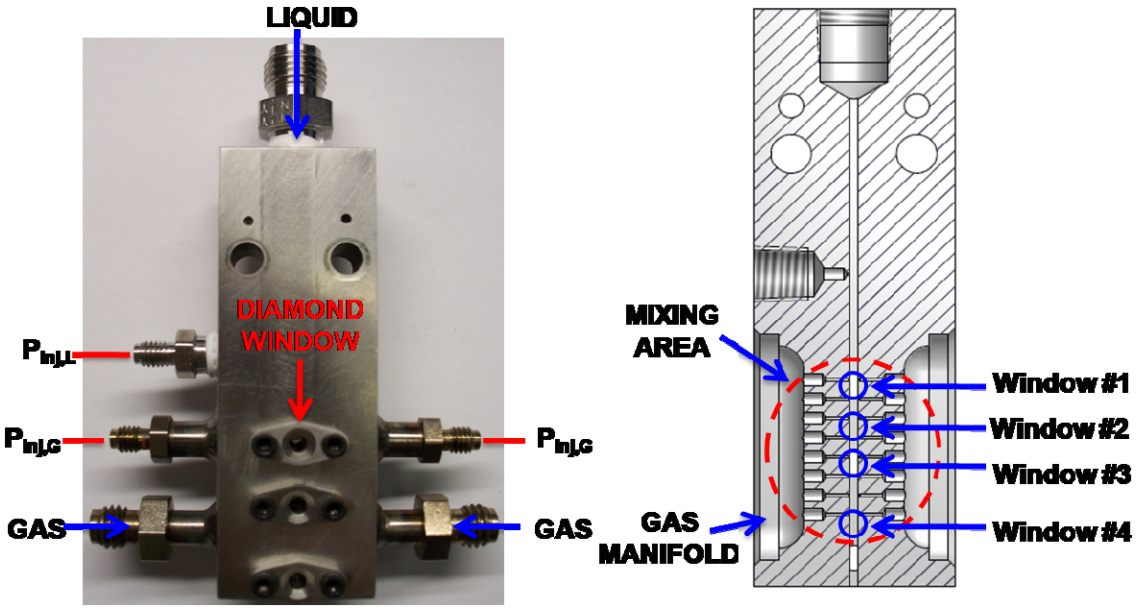

(a) (b)

Figure 1. (a) Photograph and (b) cross-sectional schematic of the rectangular aerated-liquid injector equipped with diamond windows.

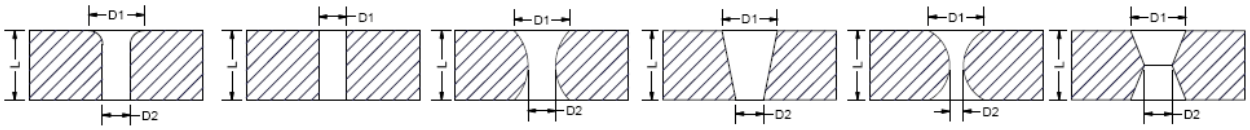

#1 #2 #3 #4 #5 #6

Figure 2. Schematics to show the adaptor internal contours for the 2.0 mm axisymmetric aerated-liquid injector. Detailed dimensions are listed in Table 1.

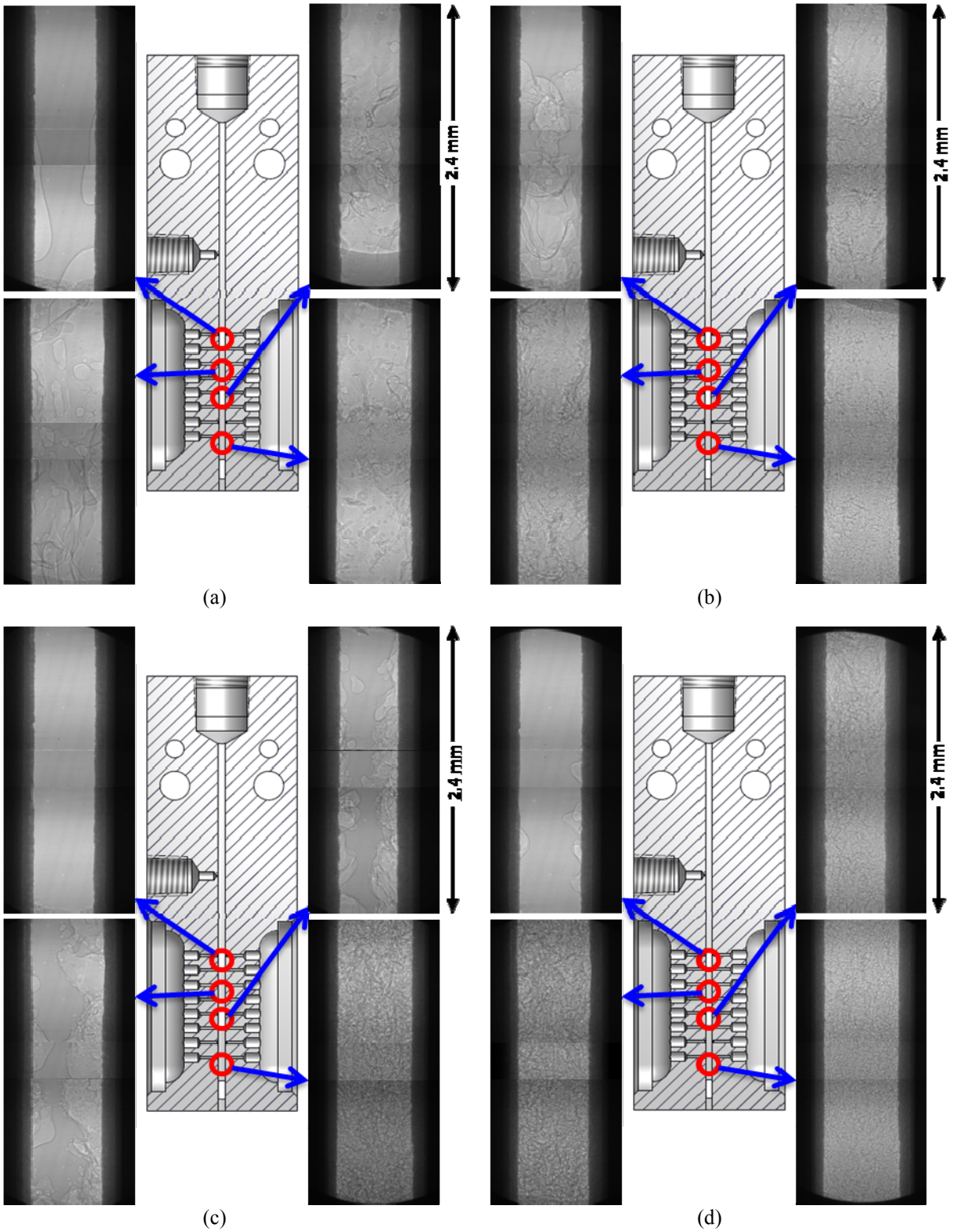

(a) (b)

(c) (d)

Figure 3. Composite x-ray images to demonstrate the evolution of two-phase mixtures inside the rectangular injector at various injection conditions. (a) Q_L=2.3 g/s, GLR=2%, $P_{ing,L}$= 0.16 MPa, $P_{inj,G}$= 0.14 MPa, (b) Q_L=2.3 g/s, GLR=8%, $P_{ing,L}$= 0.30 MPa, $P_{inj,G}$= 0.35 MPa, (c) Q_L=13.6 g/s, GLR=2%, $P_{ing,L}$= 1.15 MPa, $P_{inj,G}$= 0.91 MPa, (d) Q_L=13.6 g/s, GLR=8%, $P_{ing,L}$= 2.45 MPa, $P_{inj,G}$= 2.34 MPa.

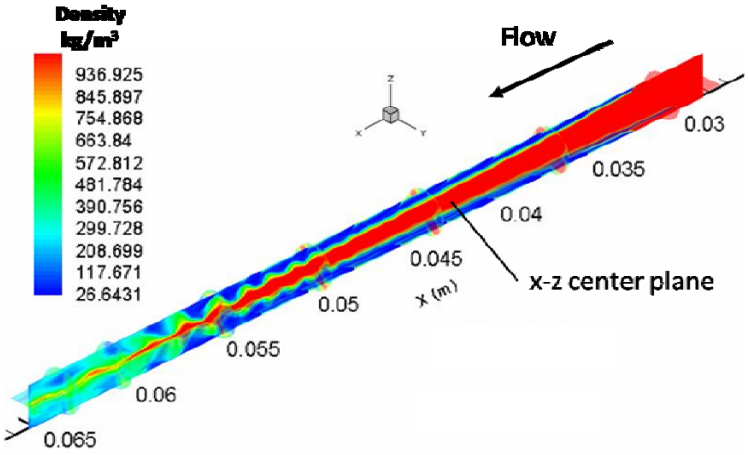

Figure 4. Numerical density contours on an x-z center plane inside an aerated-liquid injector to illustrate the internal two-phase flow structure. d=1.0 mm, Q_L=7.6 g/s, GLR=2%. From Cassidy et al. [13].

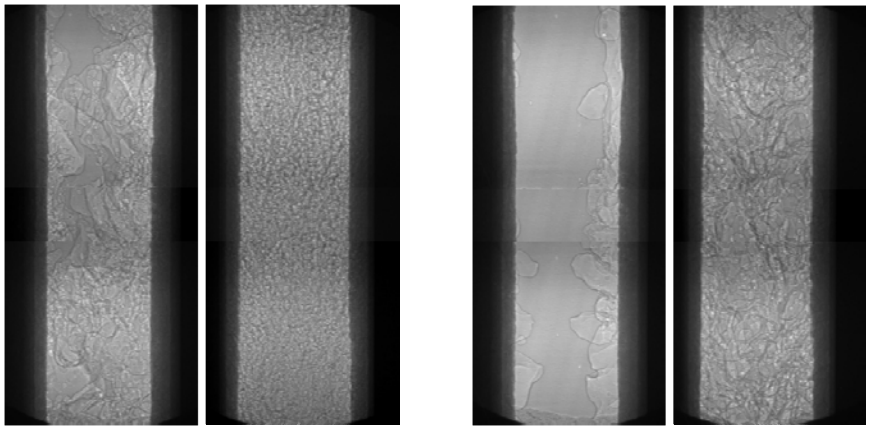

Figure 5. Composite x-ray images from two window locations to illustrate the effect of injection pressure on two-phase mixtures inside the rectangular injector. Q_L=13.6 g/s, GLR=4%. (a) No adaptor, 1.0 mm×1.0 mm exit, $P_{ing,L}$= 1.68 MPa, $P_{inj,G}$= 1.56 MPa, (b) With adaptor, 0.75 mm×0.75 mm exit, $P_{ing,L}$= 2.17 MPa, $P_{inj,G}$= 2.01 MPa.

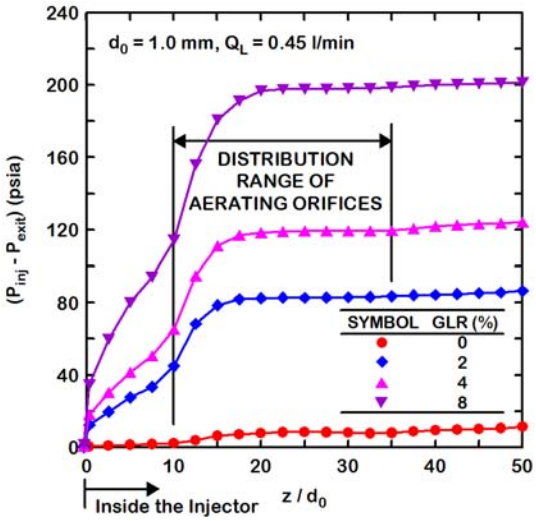

Figure 6. Pressure profiles within the aerated-liquid injector at various aeration levels. From Cassidy et al. [13].

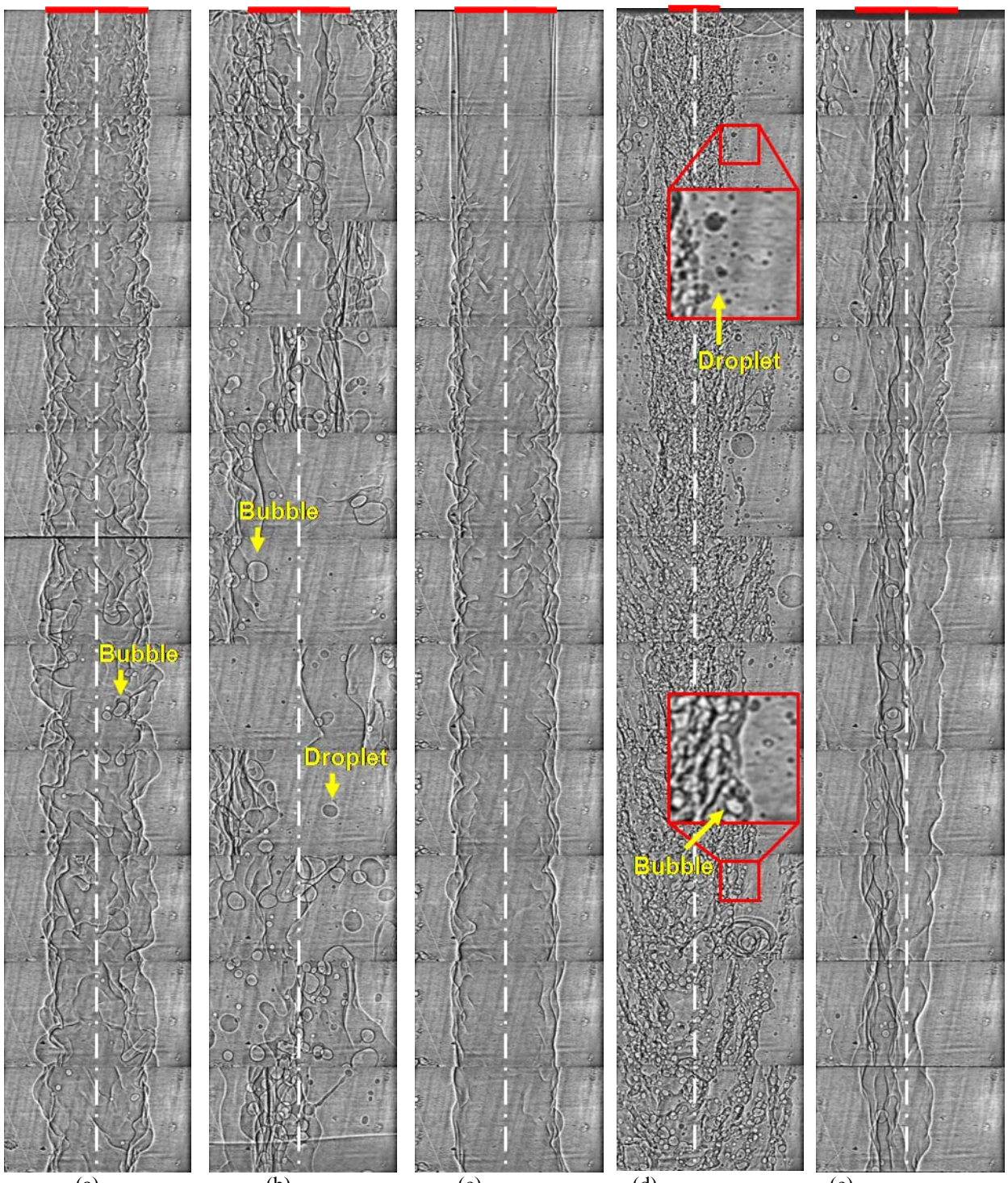

(a) (b) (c) (d) (e)

Figure 7. Contrast-enhanced composite x-ray images of aerated-liquid jets injected into a quiescent environment with various adaptors. Q_L=18.2 g/s, GLR=0, L/D=10. The physical dimension of the liquid jet in the vertical direction is 11.4 mm. (a) Configuration #1, (b) Configuration #3, (c) Configuration #4, (d) Configuration #5, (e) Configuration #6.

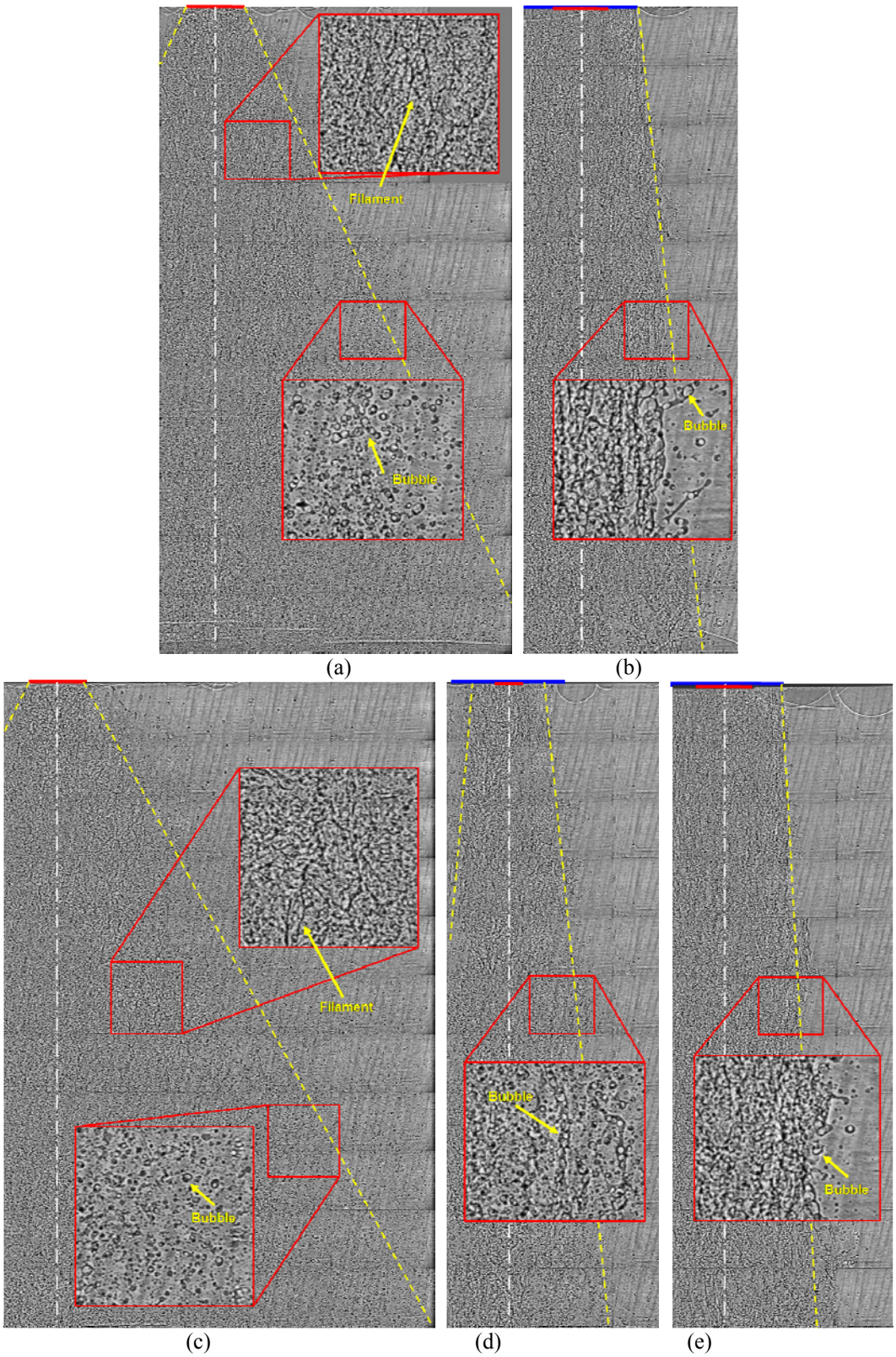

Figure 8. Contrast-enhanced composite x-ray images of aerated-liquid jets injected into a quiescent environment with various adaptors. Q_L=18.2 g/s, GLR=2%, L/D=10. The physical dimension of the liquid jet in the vertical direction is 11.4 mm. (a) Configuration #1, (b) Configuration #3, (c) Configuration #4, (d) Configuration #5, (e) Configuration #6.

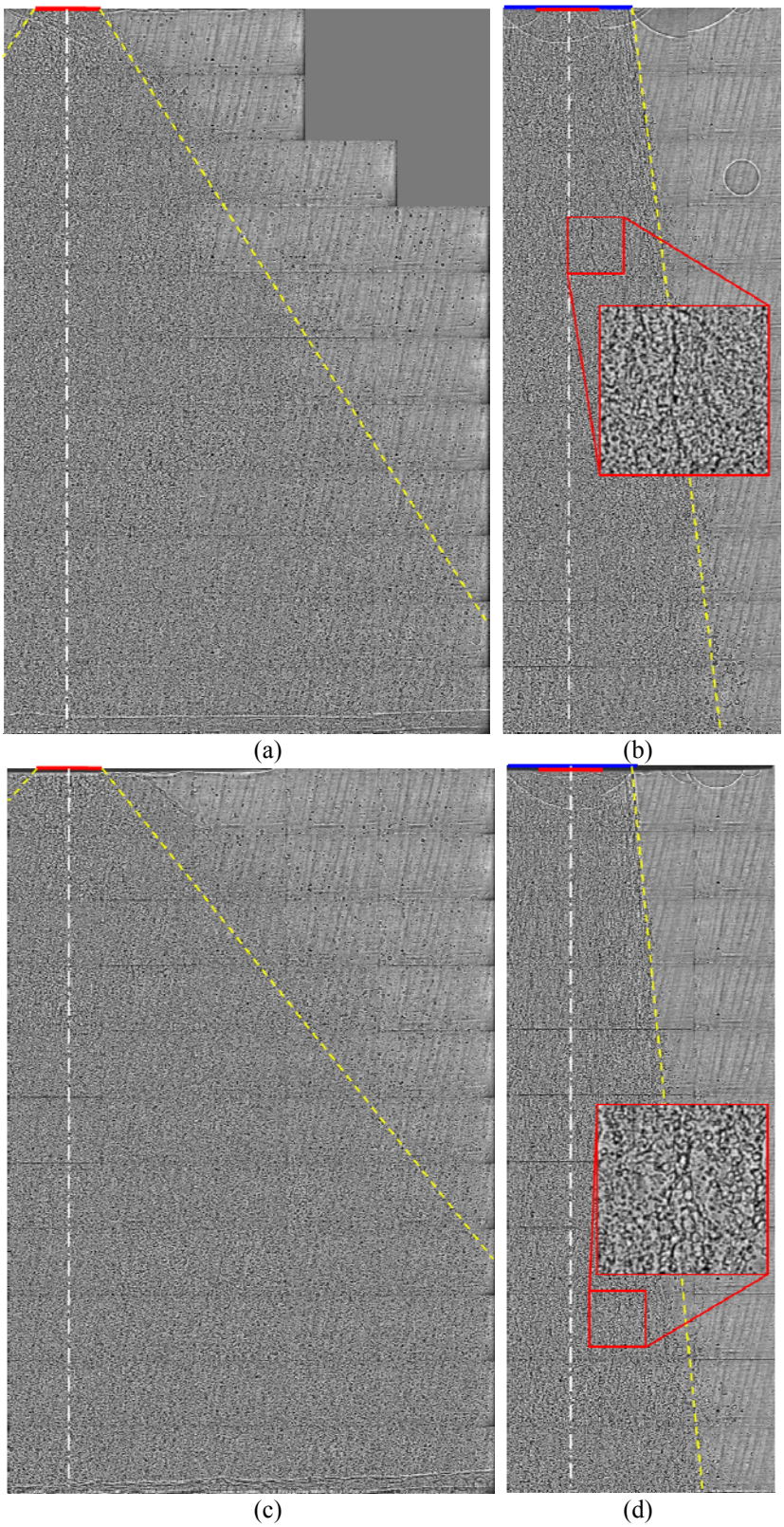

Figure 9. Composite x-ray images of aerated-liquid jets injected into a quiescent environment with various adaptors. Q_L=18.2 g/s, GLR=4%, L/D=10. The physical dimension of the liquid jet in the vertical direction is 11.4 mm. (a) Configuration #1, (b) Configuration #3, (c) Configuration #4, (d) Configuration #6.

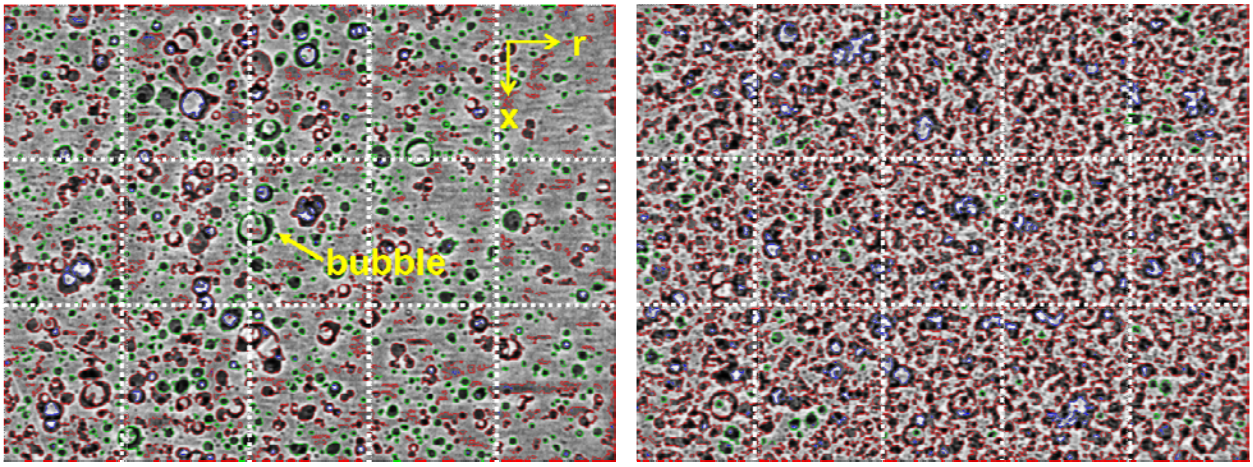

(a) (b)

Figure 10. Typical x-ray images for the measurement of droplet diameter, bubble diameter, and bubble film thickness within the aerated-liquid jets. Two-phase boundary of droplet/bubble is identified with green (external boundary) or blue (internal boundary) line. Background noise or indistinguishable object is identified with red line. Also shown are the grid lines to refine the probing resolution. Q_L=18.2 g/s, GLR=2%. Configuration #1 adaptor, L/D=10. (a) Outskirt of the spray, x=7.0 mm, r=4.2 mm. (b) Dense spray region, x=8.0 mm, r=0.

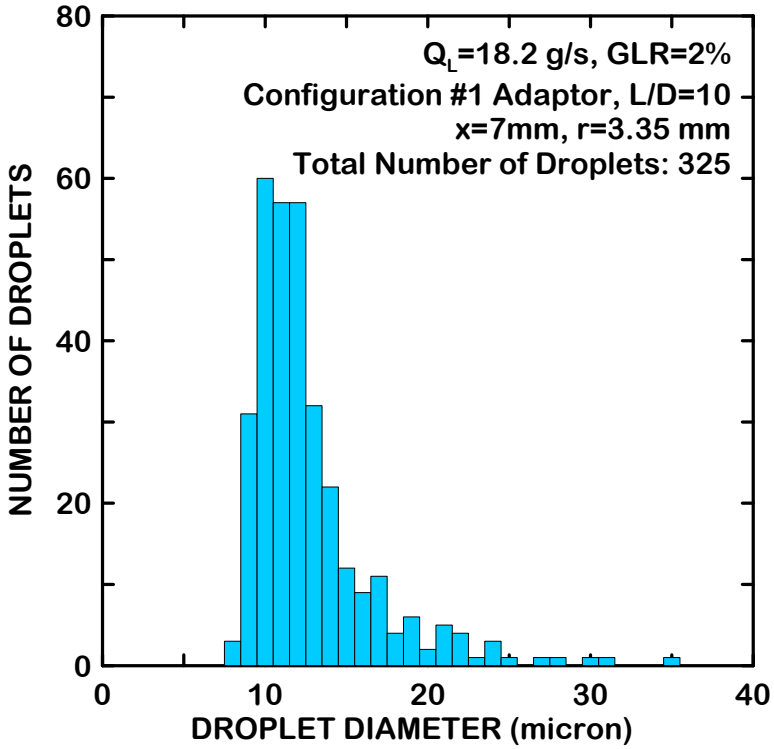

Figure 11. Typical size distribution histogram for equivalent droplet size. Q_L=18.2 g/s, GLR=2%. Configuration #1 adaptor, L/D=10, x=7.0 mm, r=3.35 mm.

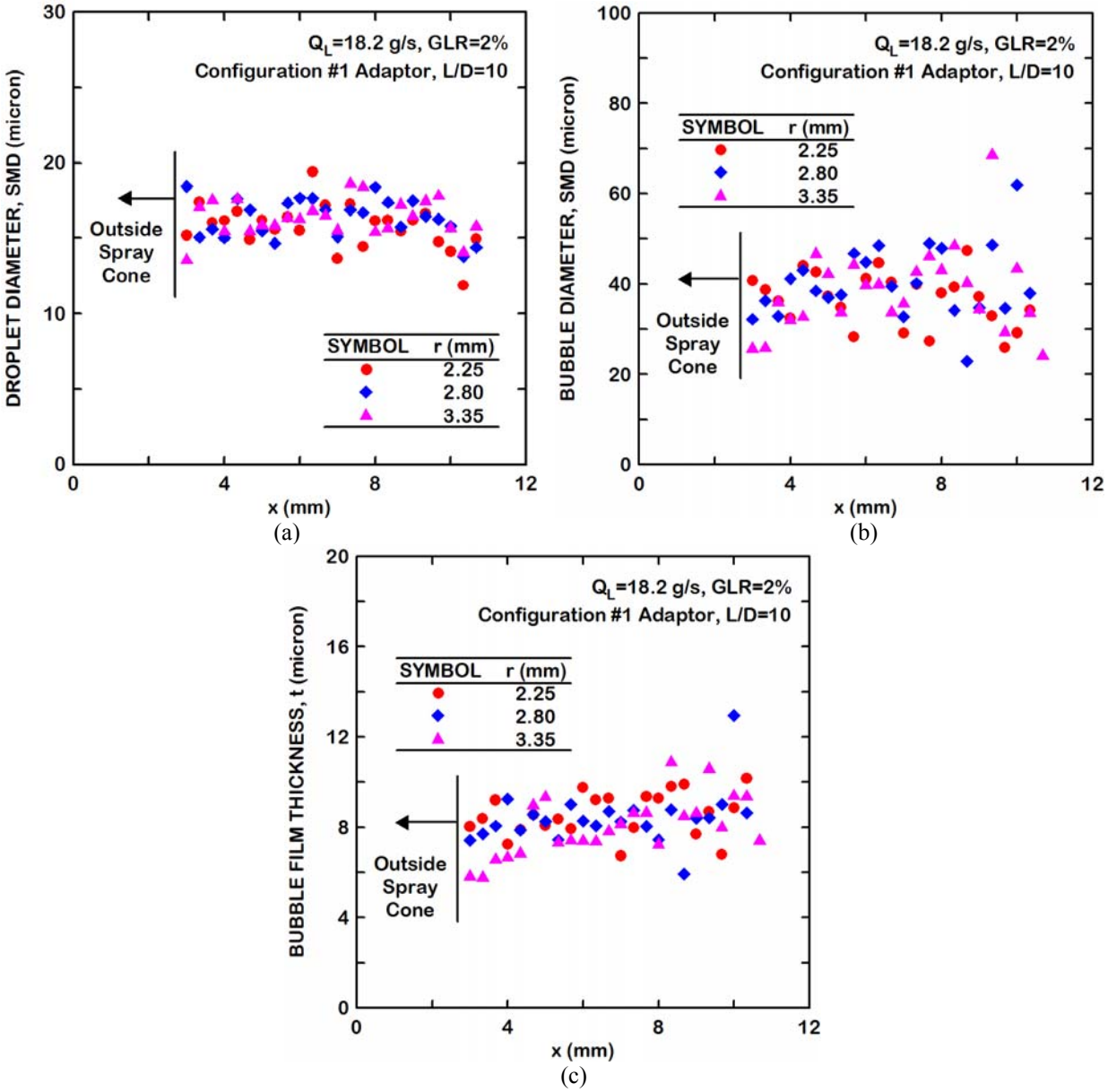

Figure 12. Size distributions along axial (x direction) line-of-sight probing paths at three radial (r direction) locations of an aerated-liquid jet. Q_L=18.2 g/s, GLR=2%, Configuration #1 adaptor, L/D=10. a) Droplet size SMD, b) Bubble size SMD, c) Bubble film thickness.

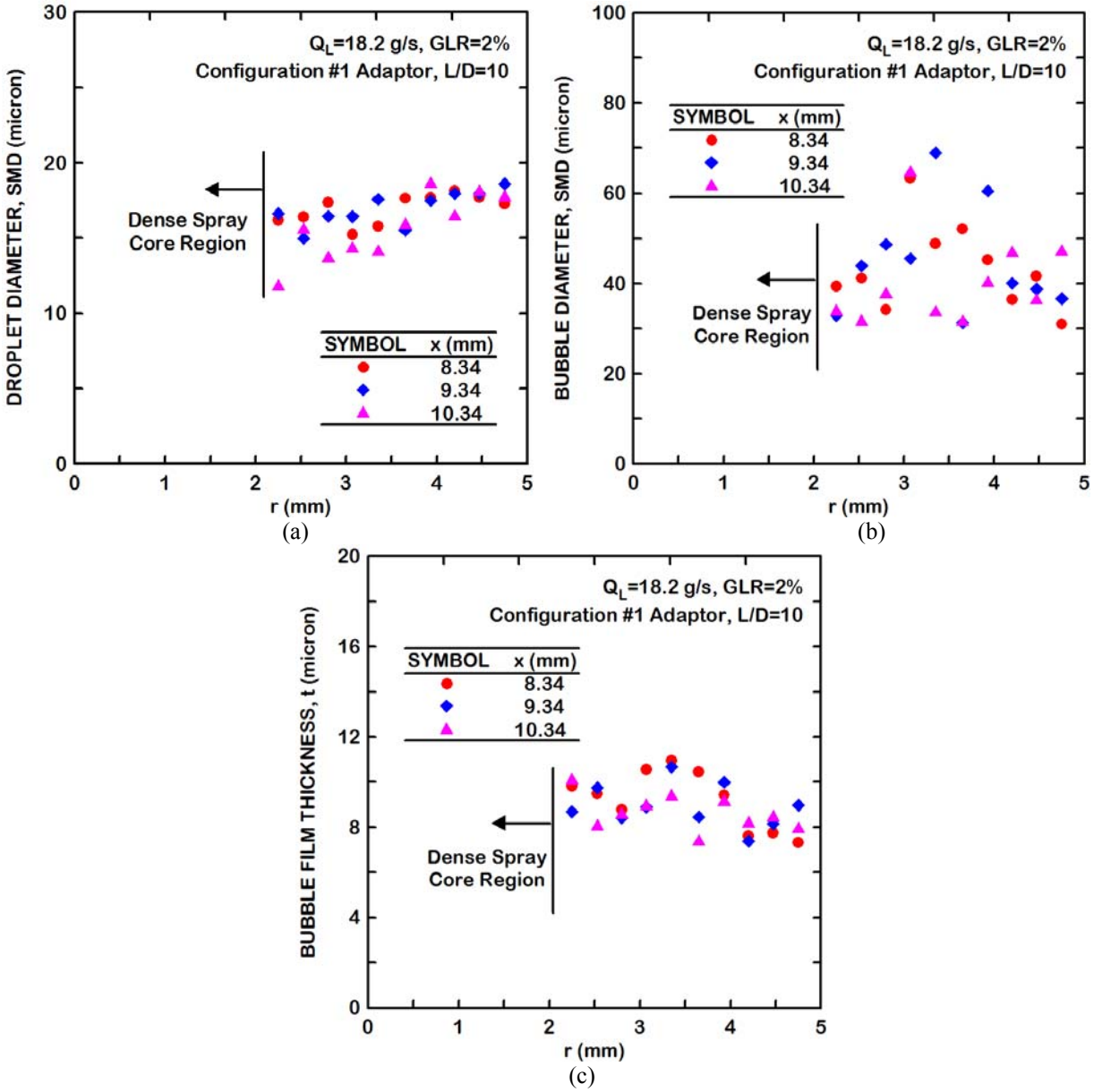

Figure 13. Size distributions along radial (r direction) line-of-sight probing paths at three axial (x direction) locations of an aerated-liquid jet. Q_L=18.2 g/s, GLR=2%, Configuration #1 adaptor, L/D=10. a) Droplet size SMD, b) Bubble size SMD, c) Bubble film thickness.